JOURNAL OF MATERIALS SCIENCE 28 (1993) 2377–2384

Basic studies of the corrosion of SiC by silicate melts

G. DRAŽIČ*, R FÖRTHMANN, A. NAOUMIDIS
Institute for Reactor Materials, Jülich Research Centre, KFA, PO Box 1913, D-5170 Jülich, Germany

Three different commercially available SiC materials (one SiSiC and two sintered SSiC) and single crystals of α-SiC were corroded at 1000 °C by silicate melts based on $Na_2O{\cdot}2SiO_2$ with different additives of Al_2O_3, CaO, Fe_2O_3 and TiO_2. During the corrosion experiments the samples were completely immersed in the melts. Parts of the samples were subsequently leached in HF for weight loss determination and surface change examinations, and other parts of them were prepared as polished cross-sections for SEM–EDXS investigations of SiC–melt interfaces. Corrosion starts by dissolution of a silicon dioxide layer in the silicate melt followed by oxidation of the free silicon phase, and silicon carbide phase, and grain boundary attack. Corrosive attack and corrosion mechanisms are dependent on the composition and structure of the silicon carbide material. An influence of Fe, Al, Ca and Ti addition on the extent of corrosion was observed. In the vicinity of SiC–melt interfaces SiO_2-rich melt regions were found. The unusually high corrosion rate of SiC samples in the case of Fe_2O_3 addition to sodium disilicate was concluded to be the consequence of Fe^{2+}–Fe^{3+} transition. Some defects in materials which were introduced during manufacturing or machining corroded much more severely than the defect-free material.

1. Introduction

Silicon carbide materials are being used increasingly for devices operating at high temperatures (heat exchangers, gas turbines etc.). Applications of SiC materials are mainly limited by their corrosion resistance in specific environments. It is known that SiC exhibits good resistance against corrosion in oxidizing atmospheres, but strongly corrodes in contact with some melts or slags.

The corrosion effects of various sodium salts (NaCl, Na_2SO_4, Na_2CO_3) on SiC at temperatures above 1000 °C have been studied and a strong influence of the melt thickness and structure of SiC on these effects has been reported [1–6]. In all cases the SiO_2 protective film reacted with molten salt, forming a sodium silicate layer. Due to a relatively fast diffusion of oxygen through this layer, SiC material was oxidized to SiO or SiO_2 (depending on the partial pressure of oxygen) at the SiC–melt interface. CO (or CO_2) which was also formed could easily diffuse from the interface due to the low viscosity of the melt. Freshly formed SiO_2 was immediately dissolved in the silicate melt until the SiO_2 enrichment of the melt was too high and a thick irregular SiO_2 tridymite film was formed on the SiC surface [3]. The corrosion of SiC by V_2O_5 and sodium silicate melt has also been investigated and reported [7, 8]. In most cases these studies were performed on SiC samples coated with a defined amount of salts (in μg cm^{-2}) where no concern was paid to the wettability of SiC surface with the melt.

Another group of published works reports on SiC corrosion by basic slags [9–11] where complicated chemical compositions of the slags were used (real or simulated residuals from coal or oil combustion. Various phases were observed such as silicates, iron silicides, SiO_2 cristobalite and tridymite that formed at the SiC–slag interface. It was concluded that the extent of corrosion is influenced by slag thickness and molar ratio of basic to acidic oxides.

The aim of our work was a detailed study of microstructural changes and reaction mechanisms during the corrosion of various qualities of SiC material by different silicate melts. The chemical composition of the melts was sodium disilicate with and without the addition of some basic or acidic oxides (Fe_2O_3, Al_2O_3, CaO, TiO_2). The quantities of added oxides were chosen from ternary phase diagrams so that the melts had melting points around 800 °C. For a homogeneous macroscopic attack of the melt on the total SiC surface the samples were completely immersed in the melt during the corrosion experiments. In this way, also, no problems exist in connection with the influence of the melt layer thickness as mentioned in the literature.

*On leave from "J. Stefan" Institute, Ljubljana, Slovenia.

0022–2461

TABLE I SiC samples used in the study

Sample abbreviation	Manufacturer	Additives	Grade
SiSiC	CESIWID, Erlangen	20% free Si	SKI
SSiC A	ESK, Kempten	0.3% Al, 1% C	HD
SSiC B	Sohio, Niagara Falls	0.5% B, 0.4% C	Hexoloy
SCSiC	ESK, Kempten		Single crystals

2. Experimental procedure

2.1. SiC materials

Three different qualities of commercially available SiC material and SiC single crystals were used for corrosion experiments. One type of material was siliconized SiC (SiSiC); the other two types were reactive-sintered SiC (SSiC) with the addition of either carbon and aluminium or boron. In Table I samples, manufacturers, grades and chemical compositions are listed.

Three different geometries of each sample were used for the different post-investigation methods. For weight loss and surface changes during corrosion bars were employed (3.5 mm × 4.5 mm × 15 mm). For cross-sections for SEM with energy-dispersive X-ray spectroscopy (EDXS) similar bars were used with a 1 mm saw-machined gap at the middle of the sample. For TEM study 150 μm thick (3.5 mm × 4.5 mm) foils were used. Prior to corrosion experiments all samples were ground with 800 grit SiC paper.

2.2. Silicate melts

Compositions of the melts were based on $Na_2O{\cdot}2SiO_2$ with the addition of various oxides. Molar ratios of oxides and abbreviations of the melts are listed in Table II. Na_2CO_3, SiO_2, Fe_2O_3, Al_2O_3, CaO and TiO_2, all from Merck (p.a. quality) were used as starting materials for melt preparation. Chemicals were mixed in platinum crucibles in the proper proportions and heated in a silite muffle furnace at 600 °C for 15 h (to decompose sodium carbonate) and at 1200 °C for 5 h. After cooling the glass was crushed in an agate mortar, fired at 1200 °C for 2 h and subsequently quenched in air and ground to powder.

2.3. Corrosion experiments and characterization of samples

Samples from each type of SiC material were placed in separate Pt crucibles, covered with powdered glass and fired in a silite muffle furnace at 1000 °C for 15 h (and for 3 h in the case of NSF melt). After firing the samples were separated from the glass using a vibrator with a diamond point. Samples in the form of bars were leached in 20% HF solution and weighed. These samples were also used for surface change examinations. Samples with the gap were embedded in Cu–epoxy resin and cross-sections were made by grinding and polishing using diamond plates and 6, 3 and 1 μm diamond pastes.

The surface corrosion effects were examined using SEM (CamScan S4DV). The chemical composition of the melt at different distances from the SiC–melt interface was measured on cross-sections using SEM–EDXS (AMR–Leitz 1600 T with PGT system IV). The total corrosion of the whole sample ("shrinkage" in μm) was measured by using a micrometer. The depth of defects (corrosion pits) at the surface of the samples was measured using optical microscopy (Leitz Metaloplan). An analytical transmission electron microscope (Jeol 2000 FX with Link AN 10000 EDXS) was also used in this study.

TABLE II Chemical compositions of melts used in experiments (in mol % oxide)

Oxide	Label				
	NS2	NSF	NSA	NSC	NST
SiO_2	67	63	61	71	63
Al_2O_3			8		
TiO_2					5
Na_2O	33	31	31	24	32
CaO				5	
Fe_2O_3		6			

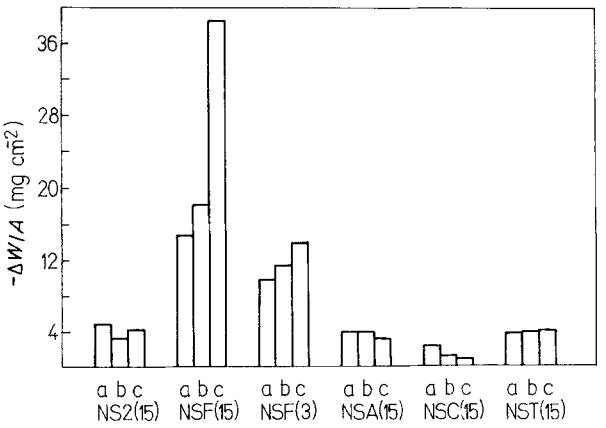

Figure 1 Weight loss of different commercial SiC samples after corrosion at 1000 °C by different sodium silicate melts (numbers in parenthesis represents corrosion time in hours): (a) SiSiC, (b) SSiC A, (c) SSiC B.

3. Results and discussion

3.1. Weight loss

The weight loss of the samples after corrosion treatment and leaching in HF as a function of the chemical composition of melts used in experiments at 1000 °C is shown in Fig. 1 (numbers in parenthesis represent corrosion time in hours). Due to the complicated geometry the surface area of the SCSiC (monocrystal)

sample could not be accurately determined, so this sample was not considered in this part of the study.

Whereas addition of Al_2O_3 (NSA melt) and TiO_2 (NST melt) to the silicate melt composition had no strong influence on the weight loss of the SiC samples, the addition of Fe_2O_3 (NSF melt) caused an extremely high loss during corrosion experiments. As can be seen from Fig. 1, during the corrosion of SiSiC and SSiC A by the NSF melt at 1000 °C more than 2/3 of the weight loss occurred within the first 3 h, while in the case of the SSiC B a strong difference was observed between weight losses after 3 and after 15 h. The weight change during corrosion by the NSC melt was relatively low, particularly for the sintered SiC types, probably because of the different composition of this silicate melt. In order to explain such differences in weight loss we performed a detailed study of the surfaces of the samples prior to and after the corrosion experiments.

3.2. Surface investigations

From the SEM micrographs of as-received samples (Fig. 2) we concluded that each type of material had some defects already present prior to corrosion experiments. The main irregularity in the SiSiC samples was a non-uniformly distributed Si phase which in some cases formed several 10 μm-wide areas. In the SSiC A samples large pores ("deep craters") and shallower "circular" defects could be seen and in the SSiC B samples pores ("deep craters") and longitudinal deep defects ("canyons"), probably arising from the forming of green bodies by extrusion, were noticed. The examined surfaces of the single crystals were without any visible defects.

As expected, the defects present in the material corrode more extensively than other, more uniform parts of the samples. The general conclusions made on the basis of the micrographs shown in Fig. 2 and the measurements of the sample dimensions and the depth of particular defects after corrosion are as follows:

1. In siliconized SiC the corrosion attack was generally more severe to the Si phase than to the SiC phase. The difference between the Si and the SiC corrosion was dependent on the melt used in the experiments. In Fig. 3 the total corrosion effect ("shrinkage") of the samples and the depth of the large Si areas in these samples are shown. It is surprising that in the case of NSA and NSC melts no corrosion of SiC phase could be measured with a micrometer, while NS2 significantly attack this phase. Therefore, the relative corrosion attack of the Si phase in comparison to the SiC was higher in the case of the NSA and NST than in the case of other melts.

2. In SSiC samples with Al and C sinter additives (SSiC A) circular defects and deep craters corroded most extensively in the case of the NSF melt as can be seen from Fig. 4. Of interest was the different corrosion behaviour of the grain boundaries in these samples. While in the case of corrosion by NS2 and NSF melts practically no grain boundaries could be seen, extensive grain boundary attack was observed in the case of NSA, NSC and NST melts (Fig. 2). Compared to SiSiC, no changes in dimensions of the SSiC A could be measured after corrosion in NSA and NSC.

3. The most severe corrosion effects were observed in SSiC B samples with sinter additives of carbon and boron Fig. 2 and Fig. 5 where some of the craters had a deepness of more than ~ 0.25 mm. In these samples no dimensional changes were observed in the case of corrosion by the NSA and NSC melts, and the highest extent of corrosion was found in the case of the NSF melt in agreement with the results on the other SiC qualities.

4. Corroded surfaces of single crystals (SCSiC) were observed in the $\langle 0001 \rangle$ direction (base planes). Beside large regular hexahedric corrosion pits which are probably due to dislocations, smaller, less regular pits were observed. The shape and dimensions of these pits were influenced by the composition of the melt (Fig. 2).

3.3. Investigations of cross-sections

Examining cross-sections we found that regarding the corrosion effects, melts could be divided into two groups. The first group, consisting of NS2 and NSF melts, corroded both phases Si and SiC in the case of SiSiC (corrosion pits were detected only in parts where large areas of Si phase were present) while the second group of the melts (NSA, NSC and NST) preferentially corroded the Si phase. In the case of corrosion of the sintered materials SSiC A and SSiC B, the second group of melts corroded more extensively the boundaries between SiC grains, which was not the case in corrosion experiments using melts from the first group. In Fig. 6 the cross-sections of examined samples corroded by NSF and NSA melts are shown.

3.3.1. EDXS microanalysis of cross-sections

Chemical compositions of the melt at different distances from the SiC–melt interface were measured using EDXS. In Fig. 7 the results of analyses for SiSiC samples corroded by NSF melt for 3 and 15 h are shown in the quasi-ternary phase diagram SiO_2–$Na_2O{\cdot}SiO_2$–Fe_2O_3. It can be seen that close to the interface the concentration of SiO_2 in the melt was raised. At the interface itself a discrete SiO_2-enriched phase was observed (dark phase at the interface in Fig. 6). Similar concentration profiles were also observed in the case of other melts and samples.

From Fig. 7 we could conclude that due to SiO_2 enrichment in the vicinity of the SiC–melt interface this melt had a much higher viscosity than the original melt and was glassy directly on the interface. This high-viscosity layer around the sample probably hindered homogenization of the melt towards the SiC material and consequently the corrosion rate decreased. For each melt we tried to estimate the thickness of such "protective layers". We plotted the chemical composition of the melt versus distance from the interface and we defined the thickness of the protective layer as the distance from the SiC–melt interface where the chemical composition passed the liquidus line for 1000 °C in the corresponding phase

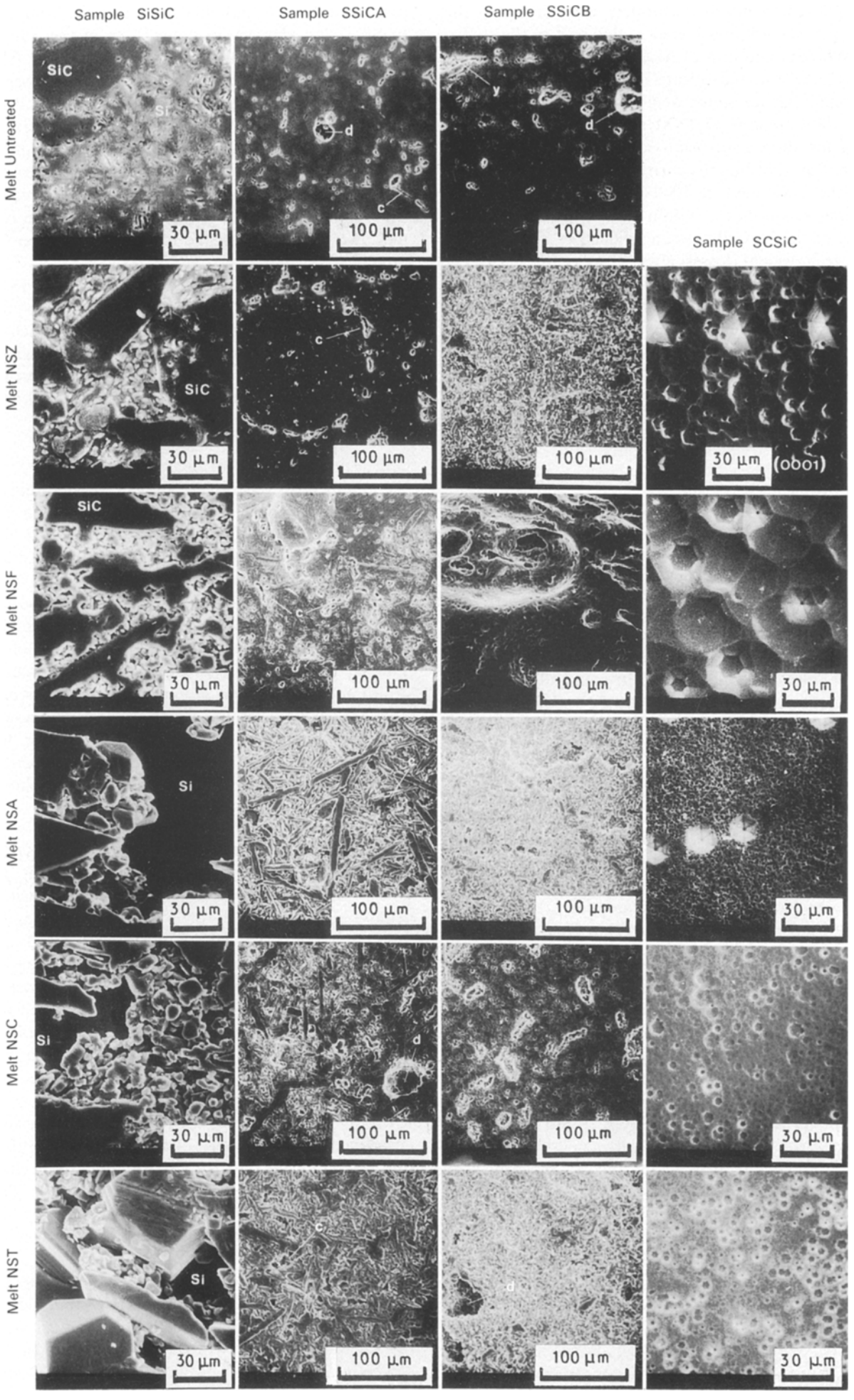

Figure 2 SEM micrographs of surfaces of samples corroded by different melts: (c) "circular defects", (d) "deep craters", (y) "canyons".

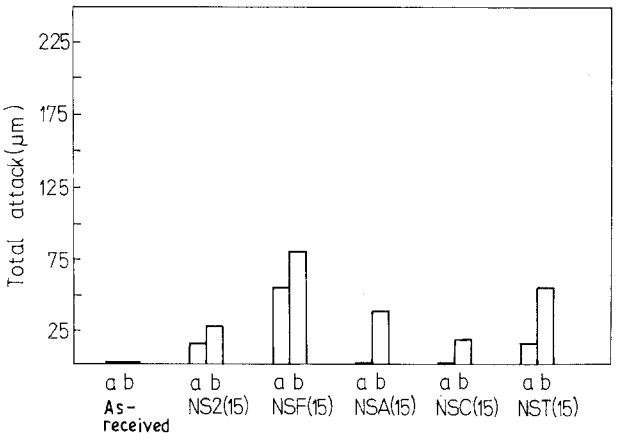

Figure 3 Corrosion attack of SiC and Si phase in SiSiC samples: (a) whole sample, (b) Si phase.

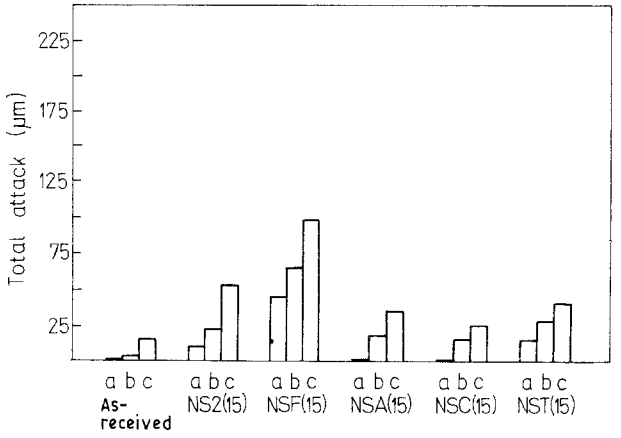

Figure 4 Corrosion attack of SiC and defects in SSiC A samples: (a) whole sample, (b) circular defects, (c) deep craters.

diagram. One should be aware that there was no direct relation between this thickness and the viscosity for different melts. In Table III the thickness of the protective layer for SiSiC samples corroded by different melts is shown.

The largest thickness of the protective layer in the case of NSC melt is in accordance with the smallest corrosion extent after 15 h as could be seen from Fig. 1. This can be explained from the Na_2O–SiO_2–CaO phase diagram [12]. The starting NSC composition (71 mol % SiO_2) is quite near to the liquidus line at 1000 °C (78 mol % SiO_2). In this case 7 mol % SiO_2 enrichment of the melt is sufficient to pass over the liquidus line. In the other cases (NSF, NSA, NST) at least 17 mol % of additional SiO_2 is necessary for the same effect.

The growth of the layer from 5 to 100 μm in the case of NSF melt for corrosion times of 3 to 15 h could explain why the corrosion rate was in the first 3 h much higher than in the following 12 hours.

The relatively small thickness of the protective layer in the case of NSA and at the same time an average corrosion extent (Fig. 1) suggested that the diffusion of oxygen through this melt is relatively slow and that the viscosity of the protective layer is extremely high.

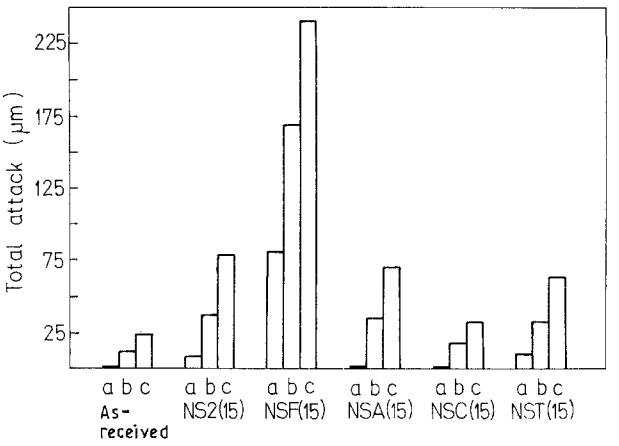

Figure 5 Corrosion attack (in μm) of SiC and defects in SSiC B samples: (a) whole sample, (b) canyons, (c) deep craters.

TABLE III Thickness of the SiO_2-rich layer on corroded SiSiC at 1000 °C

Melt[a]	NSF(3)	NSF(15)	NSA(15)	NSC(15)	NST(15)
Layer thickness (μm)	5	100	10	200	20

[a]Numbers in brackets are corrosion times in h.

The small diameters of the CO_2 bubbles and the fact that most of them are within several micrometres of the SiC–melt interface also confirmed the assumption of a large viscosity of this melt.

3.4. TEM–EDXS investigations

Using analytical TEM, no crystalline phase in the melts at the vicinity of the SiC–melt interface could be observed. At the interface amorphous, almost pure SiO_2 in 20 to 500 nm sized "drops" was found.

In Fig. 8 TEM micrographs and selected-area electron diffraction (SAED) patterns of the SiC (4H) grains and of the melt at the SiC–melt interface are shown after corrosion of SSiC A by the NSF melt at 1000° for 3 h. It was found that regions up to 500 nm large, designated G in Fig. 8, were amorphous (SAED pattern in Fig. 8b) and contained neither iron nor sodium (EDXS spectrum in Fig. 8d). On the other hand other regions of the melt (m in Fig. 8a), which were also amorphous, contained some iron and sodium beside silicon and oxygen (EDXS spectrum in Fig. 8e).

In Fig. 9a and b TEM micrographs of the SiC–melt interface of the SSiC A sample corroded by NSA melt at 1000 °C for 15 h are shown. Also in this case, pure SiO_2 amorphous phase (G), 20–50 nm large, was found at the interface. Other parts of the NSA melt (m) contained beside Si and O also Na and Al (EDXS spectrum in Fig. 9).

3.5. Corrosion by NSF melt

The observed extremely high corrosion of all samples

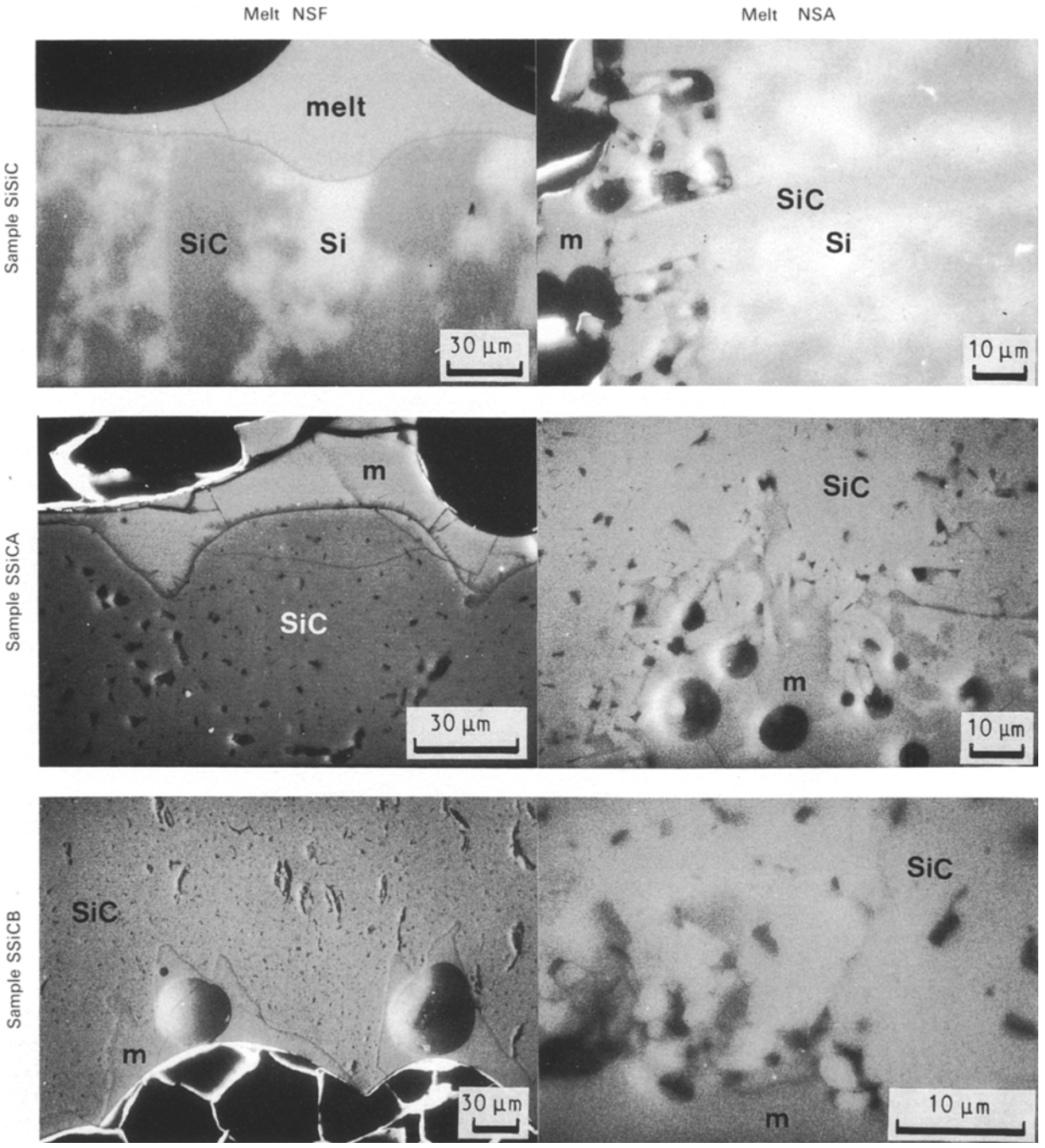

Figure 6 SEM micrographs of cross-sections of three commercial SiC samples corroded by NSF and NSA for 15 h at 1000 °C (m = melt).

by the NSF melt (Fig. 1) could be explained by the Fe^{3+}–Fe^{2+} transition in these melts. Several authors have reported [13–16] that the solubility of oxygen in silicate melts was increased if multivalent ions were added to the melt. Up to ten times larger mass flow of the oxygen through the melt was observed if just 1% of As ions was added to the melt [13].

The mechanism of oxygen diffusion in SiO_2 glass was described by Shaeffer [14] by interaction of network oxygen atoms with dissolved molecular oxygen (O_2). This dissolved molecular oxygen generates interstitial defects and acts as a carrier for the transport of network oxygen. Therefore the solubility of oxygen is dependent on the oxygen partial pressure in the oxidizing atmosphere. Diffusion in multicomponent silicate glasses is more complex. In silicate glasses the mobility of dissolved oxygen becomes higher because the chemical bond in the silicate is weaker than in pure SiO_2 and consequently the viscosity becomes lower. The presence of polyvalent metal ions reduces the dependence on oxygen partial pressure, and is controlled by the chemical solubility of oxygen which in turn is influenced by the type and concentration of polyvalent metal ions. In the case of iron ions the oxygen solubility is given by the reaction [15]

$$4Fe^{2+} + O_2(\text{glass}) \rightarrow 4Fe^{3+} + 2O^{2-}$$

In this case the oxygen partial pressure dependence is

given by $(P_{O_2})^{1/4}$. A mass transport like O_2 diffusion is no longer necessary for the oxidation of SiC. The observed higher oxidation rate may be explained by the electron transport from the SiC–melt interface through the Fe^{2+}–Fe^{3+}-containing melt to the outer surface.

We did not find any iron silicide phase at the SiC–melt interface, as reported for experiments at higher temperatures [9, 11]. Therefore we assume that the concentration of Fe ions in the SiC–melt interface is so low and the viscosity of the melt is so high that the reaction with free silicon could not take place.

The extremely high corrosion rates observed in the case of sintered SiC with boron sinter additives (SSiC B) by NSF melts was due to defects in the received samples ("canyons"), so that the active area was much higher than in the case of other samples. In this case the melt could easily penetrate quite deeply in the sample (several hundreds of micrometres).

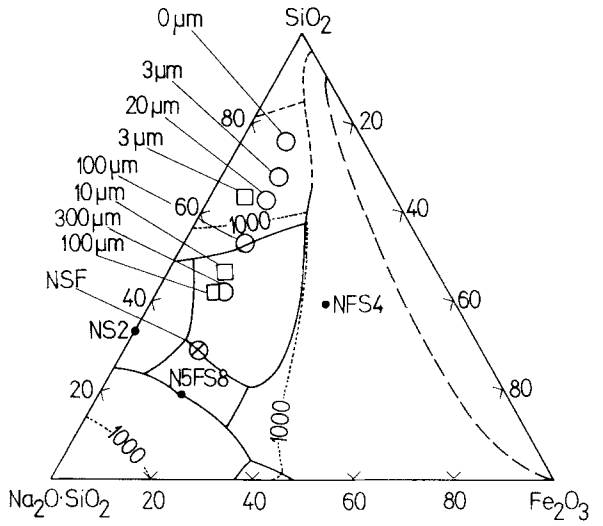

Figure 7 Quasi-ternary Na_2O–Fe_2O_3–SiO_2 phase diagram [12] containing the determined composition of the NSF melt versus distance from the SiC–melt interface for SiSiC samples after corrosion for (□) 3 and (○) 15 h at 1000 °C (NSF = starting composition of the melt).

4. Conclusions

1. Defects in starting materials (pores, cracks, chemical inhomogeneities) strongly influenced the corrosion attack of silicon carbide ceramics by molten sodium silicate at 1000 °C.

2. The addition of various oxides to $Na_2O{\cdot}2SiO_2$ melts caused different extents of corrosion of SiC materials.

3. As a corrosion product an amorphous, high-viscosity SiO_2-rich melt is formed at the SiC–melt interface which probably acts as a "protective layer". The thickness of this layer depends strongly on the chemical composition of the starting melt and on the corrosion time.

4. The extremely high corrosion rates in the case of sodium silicates with Fe_2O_3 additions were explained by the Fe^{2+}–Fe^{3+} transition which enhances electron transport through the melt and causes the high oxidation rate of silicon carbide.

Acknowledgements

This work was performed within the framework of the

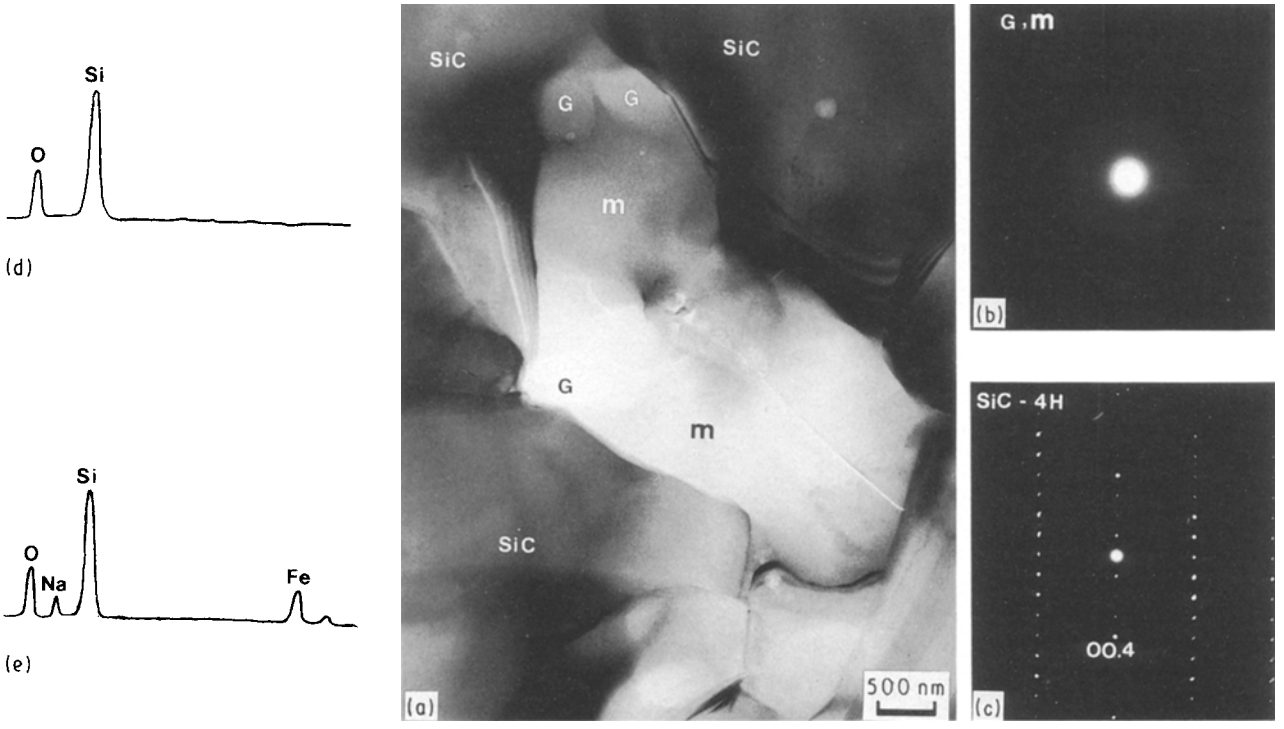

Figure 8 (a) TEM micrograph of the SiC–melt interface in SSiC A sample corroded by sodium silicate melt containing Fe_2O_3 (m = melt, G = glassy phase at the SiC–melt interface); (b) SAED pattern of m and G phase; (c) SAED pattern of SiC 4H grain; (d) EDXS spectrum of the G phase; (e) EDXS spectrum of the melt.

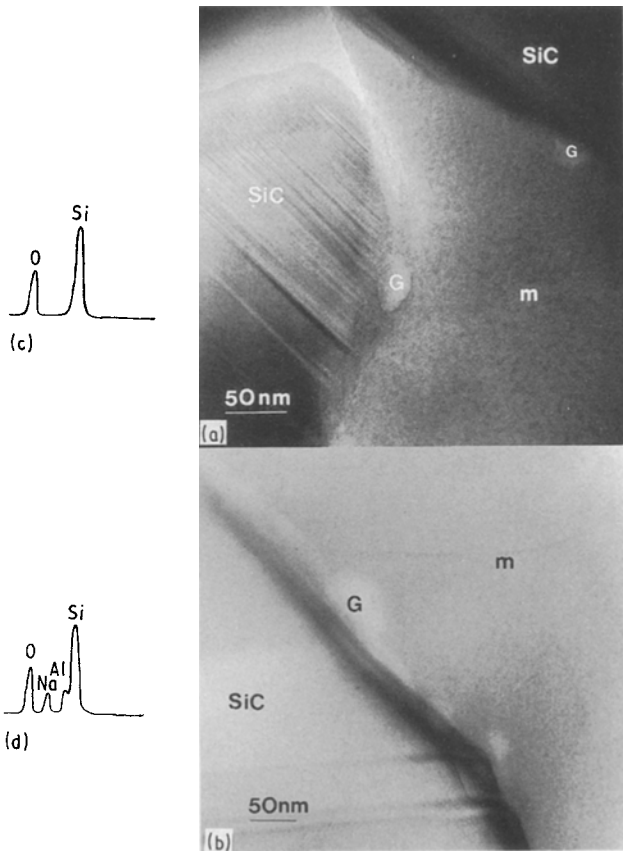

Figure 9 (a, b) TEM micrographs of the SiC–melt interface in SSiC A sample corroded by sodium silicate melt containing Al_2O_3 (m = melt, G = glassy phase); (c) EDXS spectrum of the G phase; (d) EDXS spectrum of the melt.

Bilateral Agreement between the Ministries of Research and Technology of Yugoslavia and the Federal Republic of Germany. The authors wish to thank Mrs König (SEM), Mr Blass (preparation) and Mr Hoven (metallography) for their experimental assistance.

References

1. J. I. FEDERER, *Adv. Ceram. Mater.* **3** (1988) 293.
2. *Idem, ibid.* **3** (1988) 56.
3. N. S. JACOBSON, *J. Amer. Ceram. Soc.* **69** (1986) 74.
4. N. S. JACOBSON and J. L. SMIALEC, *J. Electrochem. Soc.* **133** (1986) 2615.
5. D. W. McKEE and D. CHATTERJI, *J. Amer. Ceram. Soc.* **59** (1976) 441.
6. R. E. TRESSLER, M. D. MEISER and T. YONUSHONIS, *ibid.* **59** (1976) 278.
7. W. C. SAY, J. K. WU and W. L. CHEN, *J. Mater. Sci.* **25** (1990) 1614.
8. D. P. BUTT and J. J. MECHOLSKY, *J. Amer. Ceram. Soc.* **72** (1989) 1628.
9. M. K. FERBER, J. OGLE, V. J. TENNERY and T. HENSON, *ibid.* **68** (1985) 191.
10. P. F. BECHER, *J. Mater. Sci.* **19** (1984) 2805.
11. R. FÖRTHMANN, E. GRÜBMEIER, V. M. KEVORKIJAN and A. NAOUMIDIS, in Proceedings of 9th German–Yugoslav Meeting on Materials Science and Development, Stuttgart, April 1989.
12. E. M. LEVIN, C. R. ROBBINS and H. F. McMURDIE, in "Phase Diagrams for Ceramists" (National Bureau of Standards and American Ceramic Society, 1964).
13. R. G. C. BEERKENS and H. de WAAL, *J. Amer. Ceram. Soc.* **73** (1990) 1857.
14. H. A. SCHAEFFER, *J. Non-Cryst. Solids* **67** (1984) 19.
15. W. D. JOHNSTON, *J. Amer. Ceram. Soc.* **47** (1964) 198.
16. T. BAAK and E. J. HORNYAK, *ibid.* **44** (1961) 541.

Received 16 December 1991
and accepted 2 September 1992